

Orientation imaging of single molecules by wide-field epifluorescence microscopy

Martin Böhmer and Jörg Enderlein

Institute for Biological Information Processing I, Forschungszentrum Jülich, D-52425 Jülich, Germany

Received June 11, 2002; revised manuscript received August 29, 2002

A simple imaging method for direct determination of single-molecule orientations is presented that uses a wide-field epifluorescence microscope and a sensitive CCD camera. Imaging is performed with slight defocusing of the optics, allowing for direct determination of single-molecule orientation based on the characteristic intensity distribution of the defocused images. Exact wave-optical calculations of these defocused images are presented and are in good agreement with the measurements. These calculations represent what is to the authors' knowledge the first complete wave-optical modeling of defocused imaging of dipole emitters at an interface; the peculiarities of dipole emission at an interface and the vector effects of that emission and of imaging with a high-numerical-aperture objective are taken into account. © 2003 Optical Society of America
OCIS codes: 260.2510, 260.1960, 300.2530.

1. INTRODUCTION

Fluorescence spectroscopy of single molecules has become a routine technique with which to study the physical and chemical behavior of individual molecules and has become an increasingly important tool for molecular biology (for a recent overview of the field see Ref. 1). A topic of special interest has always been the experimental determination of the spatial orientation of the molecule's absorption-emission dipole. Information about this orientation is important for several reasons: On the one hand, photophysical parameters of single molecules, such as fluorescence lifetime and observable emission intensity, often depend on the orientation of the molecules. On the other hand, single-molecule orientation can itself be a probe for studying the photophysics of the molecule^{2,3} or the structure of its environment^{4,5} or for probing the orientation of labeled biomolecules.⁶⁻¹⁰ In the past, several techniques were used for determining single-molecule orientations by fluorescence measurements. In what follows, we summarize only the research that was performed at room temperature and under ambient conditions. The two most popular techniques are polarization-resolved scanned imaging of single molecules with either a near-field¹¹⁻¹⁹ or a confocal far-field microscope.²⁰⁻²³ The core idea of these methods is to detect the fluorescence in two detection channels with crossed polarizers, to modulate the excitation polarization, or both. In particular, modulation of the excitation polarization yields a highly precise determination of the in-plane orientation (perpendicular to the optical axis) of the absorption dipole moment. When more-sophisticated data analysis methods are applied, even complete three-dimensional orientations of both the absorption and the emission dipoles can be obtained from such measurements.^{22,24} Variations of this method use annular excitation,²⁵ annular excitation and detection,²⁶ or excitation with radially polarized light beams²⁷ for better addressing molecule orientations along the optical axis. A third and different approach for detecting single-

molecule orientations is based on direct fluorescence imaging. The core idea of this approach is to obtain information about the angular distribution of a single molecule's fluorescence emission by causing the image of the molecule to deteriorate, either by introducing aberration²⁸⁻³⁰ or by defined image defocusing.^{31,32} In both cases, the intensity distribution of the blurred image contains information about the molecule's emission dipole orientation. The defocusing method was proposed in Refs. 31 and 32 and was experimentally demonstrated for an immersion mirror objective used for imaging within a cryostat at low temperature. Here we show that this concept is easily extended to imaging of surface-bound molecules by use of a conventional CCD-imaging epifluorescence microscope with laser wide-field illumination. We show how to calculate exactly the images of single-dipole emitters for such a system, taking into account the defocusing as well as the significant changes of the dipole emission at an interface. We present experimental results for dye molecules adsorbed at an air-glass interface. The experimental method is easily implemented and allows for fast screening of single-molecule orientations without the necessity for scanning or of excitation modulation. Thus it will be of great use for any application for which single-molecule orientations constitute an important measurement parameter.

2. THEORY

The starting point of our considerations is the emission characteristics of an electric dipole. The emission geometry is depicted in Fig. 1. For an oscillating electric dipole with amplitude vector \mathbf{p} in a medium with refractive index n_0 and distance $|z_0|$, $z_0 < 0$, above a planar interface ($z = 0$) of a dielectric with refractive index n , the electric field amplitude at position $z > 0$ within that dielectric can be given by the plane-wave representation (see, e.g., Refs. 33 and 34)

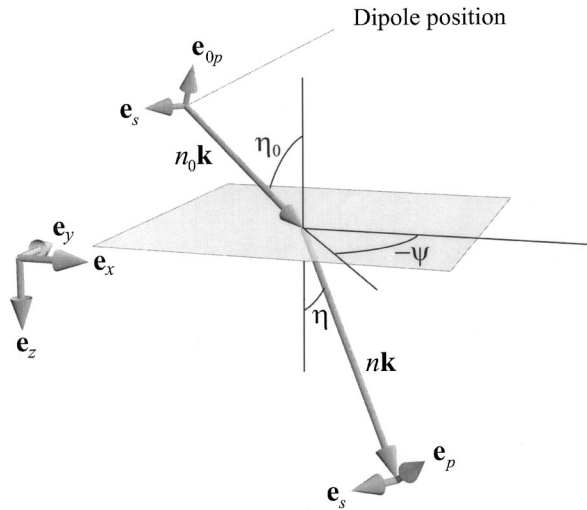


Fig. 1. Geometry of the dipole emission above an interface. The dipole emission can be thought of as a superposition of plane waves, each with a specific polarization and amplitude. At the interface, each of these plane-wave components is reflected and transmitted. The complete emission into the lower dielectric is given by the superposition of the transmitted plane waves.

$$\mathbf{E} = \frac{ik_0^2}{2\pi} \iint \frac{d\mathbf{q}}{w_0} [\mathbf{e}_p T_p (\mathbf{e}_{0p} \cdot \mathbf{p}) + \mathbf{e}_s T_s (\mathbf{e}_s \cdot \mathbf{p})] \times \exp[i\mathbf{q} \cdot (\boldsymbol{\rho} - \boldsymbol{\rho}_0) + iw_0|z_0| + iwz]. \quad (1)$$

where $(\boldsymbol{\rho}_0, z_0)$ and $(\boldsymbol{\rho}, z)$ are the coordinates of the dipole and the target point where the electric field is to be computed, respectively; w and w_0 are the z components of the wave vectors of the plane waves, $w = (n^2 k_0^2 - \mathbf{q}^2)^{1/2}$ and $w_0 = (n_0^2 k_0^2 - \mathbf{q}^2)^{1/2}$; the unit vectors \mathbf{e}_{0p} , \mathbf{e}_p , and \mathbf{e}_s are the p - and s -polarization vectors that are transversal to the plane-wave propagation:

$$\begin{aligned} \mathbf{e}_{0,p} &= (\cos \psi \cos \eta_0, \sin \psi \cos \eta_0, -\sin \eta_0), \\ \mathbf{e}_p &= (\cos \psi \cos \eta, \sin \psi \cos \eta, -\sin \eta), \\ \mathbf{e}_s &= (-\sin \psi, \cos \psi, 0); \end{aligned} \quad (2)$$

k_0 is the vacuum wave vector of the emitted light; $T_{p,s}$ are usual Fresnel transmission coefficients³⁵ for plane p and s waves incident at angle η_0 with respect to the z axis; and the angles η_0 and η are connected by Snell's law, $n \sin \eta = n_0 \sin \eta_0$. Two-dimensional vector \mathbf{q} is the integration variable over which the integration in Eq. (1) has to be performed, and the integration extends over the complete \mathbf{q} plane.

When one considers that any plane-wave component in Eq. (1) carries an energy proportional to the square electric field amplitude of the corresponding component, it is straightforward to obtain from Eq. (1) the angular distribution of radiation of the dipole emission into the dielectric. Moreover, because only plane-wave components with purely imaginary exponents in Eq. (1) contribute to the far-field emission, one has to consider only components with $|\mathbf{q}| \leq n k_0$. Concerning the orientation of the dipole, two different cases have to be considered: dipole orientation vertical to the interface and dipole orientation parallel to the interface.

For the vertical dipole orientation, evaluation of Eq. (1) leads to the following dependence of the electric-field amplitude on the emission angle:

$$\mathbf{E}_p^\perp(\eta) = \mathbf{e}_p E_p^\perp(\eta) = -\mathbf{e}_p \frac{n w q}{n_m w_m} T_p \exp(i w_m |z_m|), \quad (3)$$

where it was taken into account that $\sin \eta d\eta$ is equal to $q dq/nw$. Thus the electric field of the vertical dipole depends only on polar angle η and is, in all directions, polarized along \mathbf{e}_p . For the parallel dipole orientation, the angular distribution also depends on azimuthal angle ψ between the dipole orientation and the direction of emission. Again, by evaluating Eq. (1) one finds that there are two parts that depend on ψ as $\cos \psi$ and as $\sin \psi$. These two components are denoted $\mathbf{e}_p E_p^\parallel(\eta) \cos \psi$ and $\mathbf{e}_s E_s^\parallel(\eta) \sin \psi$ and are given by

$$\begin{aligned} \mathbf{e}_p E_p^\parallel(\eta) \cos \psi &= \mathbf{e}_p \frac{n w}{n_m} T_p \exp(i w_m |z_m|) \cos \psi, \\ \mathbf{e}_s E_s^\parallel(\eta) \sin \psi &= -\mathbf{e}_s \frac{n w}{w_m} T_s \exp(i w_m |z_m|) \sin \psi. \end{aligned} \quad (4)$$

After the angular distribution of the dipole emission into the glass has been found, the next step is to find an expression for the way in which this emission is imaged onto the chip of a detector CCD camera.

The imaging geometry is shown schematically in Fig. 2. It is assumed that the camera is positioned at the design back focal plane (image plane) of the imaging optics (consisting of the objective and a tube lens) and that the imaging optics is perfectly free of aberration when an object lying within the design focal plane is imaged into the conjugated design image plane. As was shown in Ref. 36, the electric and magnetic field amplitudes can then be found from the general theory developed by Richards and Wolf³⁷ for the imaging properties of optical systems with high numerical aperture. The core idea is to develop the electric and magnetic field amplitudes in image space into a superposition of plane waves and to find a connection between the plane-wave amplitudes and polarizations and the intensity and polarization of the light incident onto the objective. Following Ref. 36, the electric- and magnetic-field amplitudes for the vertical dipole are then given by

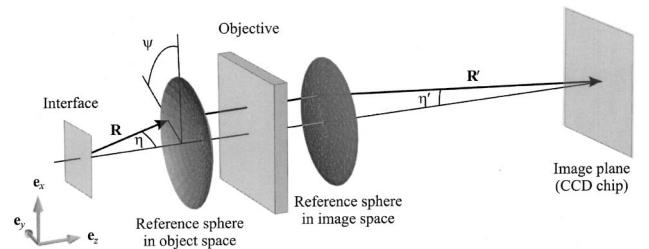


Fig. 2. Geometry of the imaging from the interface onto the CCD camera. The camera is positioned directly in the design image plane of the optics. For ideally aplanatic optics, a spherical wave front of a point source at the focus of the optics in object space is converted into a spherical wave front converging toward the conjugated focus in image space.

$$\begin{aligned} \mathbf{E} &= M \iint_{\Omega} d\Omega' \left(\frac{n' \cos \eta'}{n \cos \eta} \right)^{1/2} \mathbf{e}'_p E_p^\perp \exp(ik' \mathbf{s}' \cdot \mathbf{r}' + ik \delta z \cos \eta), \\ \mathbf{B} &= Mn' \iint_{\Omega} d\Omega' \left(\frac{n' \cos \eta'}{n \cos \eta} \right)^{1/2} \mathbf{e}'_s E_p^\perp \exp(ik' \mathbf{s}' \cdot \mathbf{r}' + ik \delta z \cos \eta), \end{aligned} \quad (5)$$

where all primed variables refer to the image space; \mathbf{r}' is the coordinate of the target point in image space where the amplitudes are calculated, n' is the refractive index of the imaging medium, usually that of air, and M is the imaging magnification. The following vectors were introduced:

$$\begin{aligned} \mathbf{e}'_p &= (\cos \psi \cos \eta', \sin \psi \cos \eta', -\sin \eta'), \\ \mathbf{s}' &= (-\cos \psi \sin \eta', -\sin \psi \sin \eta', \cos \eta'). \end{aligned} \quad (6)$$

The integration extends over the angular space $\Omega = (\eta', \psi)$; ψ varies from 0 to 2π and η' varies from 0 to η'_{\max} . The connection between η and η' is given by Abbe's sine condition, $n \sin \eta = Mn' \sin \eta'$, so η'_{\max} is determined as $\eta'_{\max} = \arcsin(\text{NA}/Mn')$, where NA denotes the numerical aperture of the objective. The factor $M(n' \cos \eta'/n \cos \eta)^{1/2}$ ensures that energy is conserved on imaging. In addition to the notation introduced in Ref. 36, in Eqs. (5) the exponential factor $ik \delta z$ is introduced, accounting for a possible axial shift δz between the design focal plane of the objective and the medium-glass interface, which will be significant in our discussion below.

An analogous result holds for the parallel dipole orientation, which reads explicitly as

$$\begin{aligned} \mathbf{E} &= M \iint_{\Omega} d\Omega' \left(\frac{n' \cos \eta'}{n \cos \eta} \right)^{1/2} (\mathbf{e}'_p E_p^\parallel \cos \psi + \mathbf{e}'_s E_s^\parallel \sin \psi) \exp(ik' \mathbf{s}' \cdot \mathbf{r}' + ik \delta z \cos \eta), \\ \mathbf{B} &= Mn' \iint_{\Omega} d\Omega' \left(\frac{n' \cos \eta'}{n \cos \eta} \right)^{1/2} (\hat{\mathbf{e}}'_s E_p^\parallel \cos \psi - \mathbf{e}'_p E_s^\parallel \sin \psi) \exp(ik' \mathbf{s}' \cdot \mathbf{r}' + ik \delta z \cos \eta). \end{aligned} \quad (7)$$

Next, the product $\mathbf{s}' \cdot \mathbf{r}'$ can be expanded as

$$\begin{aligned} \mathbf{s}' \cdot \mathbf{r}' &= \mathbf{s}' \cdot (\mathbf{R}' + \boldsymbol{\rho}' + \mathbf{z}') \\ &= R' - \rho' \sin \eta' \cos(\psi - \phi') + z' \cos \eta', \end{aligned} \quad (8)$$

where R' is the axial distance of the optics' focus from some reference plane in image space and (ρ', ϕ', z') are the cylindrical coordinates of the target point. Now, the integrations over ψ can be performed explicitly, leading to the final result that

$$\begin{aligned} \begin{Bmatrix} E_j \\ B_j \end{Bmatrix} &= M \int_0^{\eta'_{\max}} d\eta' \sin \eta' \left(\frac{n' \cos \eta'}{n \cos \eta} \right)^{1/2} \begin{Bmatrix} e_j \\ b_j \end{Bmatrix} \\ &\times \exp(ik' z' \cos \eta' + ik \delta z \cos \eta), \end{aligned} \quad (9)$$

where one finds for the vertical dipole orientation

$$\begin{Bmatrix} e_x \\ e_y \end{Bmatrix} = i \cos \eta' J_1 E_p^\perp \begin{Bmatrix} \cos \phi' \\ \sin \phi' \end{Bmatrix},$$

$$\begin{Bmatrix} b_x \\ b_y \end{Bmatrix} = in' J_1 E_p^\perp \begin{Bmatrix} -\sin \phi' \\ \cos \phi' \end{Bmatrix}, \quad (10)$$

and for the parallel orientation

$$\begin{aligned} \begin{Bmatrix} e_x \\ e_y \end{Bmatrix} &= \frac{i}{2} \\ &\times \begin{Bmatrix} \cos \eta' (J_0 - J_2 \cos 2\phi') E_p^\parallel + (J_0 + J_2 \cos 2\phi') E_s^\parallel \\ -\cos \eta' J_2 \sin 2\phi' E_p^\parallel + J_2 \sin 2\phi' E_s^\parallel \end{Bmatrix}, \\ \begin{Bmatrix} b_x \\ b_y \end{Bmatrix} &= \frac{in'}{2} \\ &\times \begin{Bmatrix} -\cos \eta' J_2 \sin 2\phi' E_s^\parallel + J_2 \sin 2\phi' E_p^\parallel \\ \cos \eta' (J_0 + J_2 \cos 2\phi') E_s^\parallel + (J_0 - J_2 \cos 2\phi') E_p^\parallel \end{Bmatrix}. \end{aligned} \quad (11)$$

$J_{0,1,2}$ are Bessel functions of the first kind,³⁸ with functional argument $k' \rho' \sin \eta'$. Finally, the position-dependent detectable light intensity on the CCD camera is given by the z component of the Poynting vector:

$$S = (c/8\pi) \mathbf{e}_z \cdot (\mathbf{E} \times \mathbf{B}^*), \quad (12)$$

where one has to use the results that are found for the electric and magnetic fields of either the vertically or the parallel oriented dipole. If the emitting dipole has an intermediate orientation, i.e., has an inclination angle θ toward the surface, the electric and magnetic fields are given by $\mathbf{E} = \mathbf{E}^\perp \sin \theta + \mathbf{E}^\parallel \cos \theta$ and $\mathbf{B} = \mathbf{B}^\perp \sin^2 \theta + \mathbf{B}^\parallel \cos \theta$, respectively, where the superscripts \perp and \parallel refer to the vertical and parallel oriented dipoles.

3. EXPERIMENT

The experimental system consisted of an inverted microscope (IX70, Olympus) equipped with a 1.4-N.A., $60\times$ oil immersion objective (Planapo, infinity corrected, 0.170 cover slide corrected) and a highly sensitive Peltier-cooled CCD camera (CoolSnap HQ, Roper Scientific). Wide-field illumination for fluorescence excitation was accomplished with the light of an Ar-Kr-ion laser (Stability 2018, Spectra-Physics) at 647.1 nm with an additional excita-

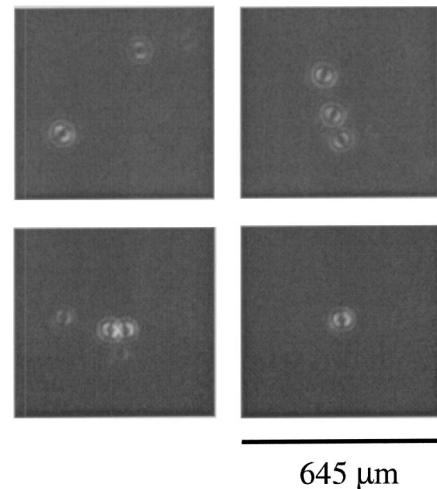


Fig. 3. Detected images of single Cy5 molecules deposited upon glass in air at a defocusing value of $-1 \mu\text{m}$ (displacement of the objective toward the sample).

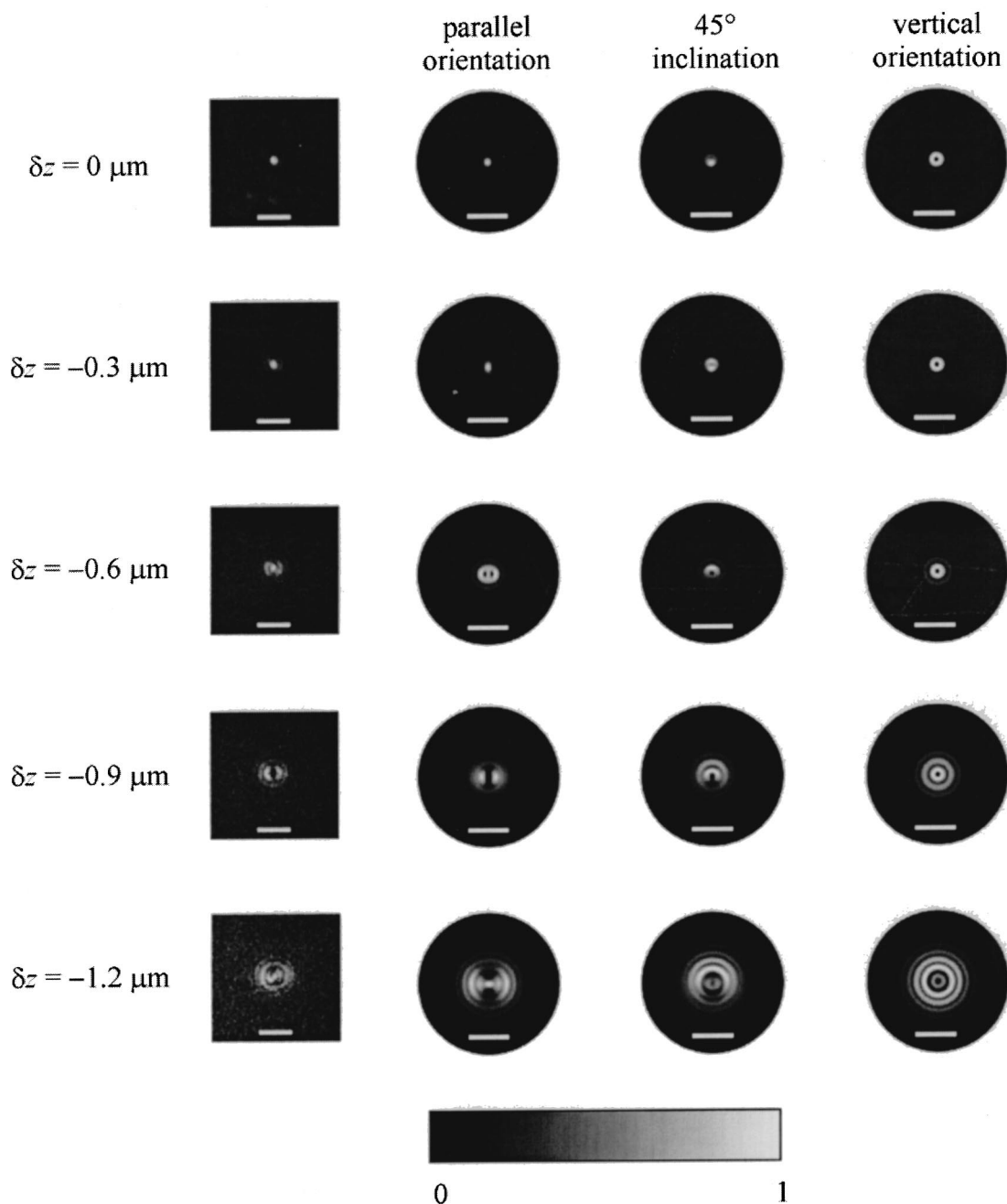


Fig. 4. Comparison of, left to right, measured images of a single molecule and theoretically calculated images for three different dipole orientations as marked and for the defocusing values indicated at the left. The white scale bars have a length of $100 \mu\text{m}$. The correspondence between intensity and gray value is shown by the gray scale at the bottom. The calculations were made for a 1.4-N.A. oil immersion objective with $60\times$ magnification imaging dipoles at an air-glass interface.

tion laser line filter (647NB4) within the excitation path. Excitation light was focused into the back focal plane of the objective (Köhler illumination mode) for achieving maximum homogeneous wide-field illumination of the sample. Circular excitation light polarization was achieved by use of a polychromatic Fresnel rhomb (FR600QM, Thorlabs) as a $\lambda/4$ phase element for elliptically polarizing the light to compensate for the polarization-dependent reflectivity of the subsequent dichroic mirror. This mirror (650DLRP, Omega Optical) served to reflect the excitation light into the back aperture of the objective. Fluorescence was collected by the

same objective and was passed through the dichroic mirror and an additional emission filter (690DF40, Omega Optical) for further background suppression (Raman-Rayleigh scattering). The CCD camera was positioned exactly at the intermediate image plane of the microscope side port. The objective was axially positioned with a piezoelectric transducer (PiFoc P-721-20, Physik Instrumente) with subnanometer resolution.

The sample that we studied consisted of standard microscope cover slides (Menzel) of $170\text{-}\mu\text{m}$ thickness, on top of which a diluted 10^{-9} M solution of the cyanine dye Cy5 (Amersham) in methanol was spin coated, yielding a

sparse distribution of single Cy5 molecules at an air-glass interface. Images of the sample were taken with an exposure time of 3 s. We adjusted the image focusing by stepwise moving the objective with the piezoelectric transducer until we achieved diffraction-limited images of the molecules. Next, the position of the objective was moved by as much as 1.2 μm toward the sample for image defocusing.

4. RESULTS

Typical measured images of single molecules obtained for a defocusing value of $\delta z = -1 \mu\text{m}$ are shown in Fig. 3. The images show a distinctive bipolar pattern that corresponds to emitting dipoles with orientation parallel to the surface. We screened images of ~ 100 molecules, and all showed the same emission pattern. This result confirms earlier reports for a mostly parallel orientation of transition dipoles for molecules adsorbed directly onto a glass surface (see, e.g., Ref. 22).

For comparison of experimental results with theoretical calculations, a series of five images was taken with increasing defocusing values ranging from 0 to 1.2 μm in steps of 300 nm. Because of the long exposure time of 3 s, only a few molecules survived all exposures without photobleaching or blinking. The images for such a rare event are shown in the leftmost photographs in Fig. 4. The remaining columns of photographs, from left to right, show the calculated images for parallel, inclined, and vertical dipole orientation. The calculations exploited Eqs. (9)–(12) for determining the energy flow distribution through the image plane and thus the intensity distribution as seen by the CCD detector. The refractive indices used in the calculations were $n_0 = 1.0$, $n = 1.51$, and $n' = 1.0$; magnification M was set to 60; and the numerical aperture was 1.4.

A fair correspondence between the measured images and the patterns calculated for the parallel dipole orientation can be seen. Obviously, the in-plane orientation of the measured molecule is nearly along the vertical figure axis, and the parallel-dipole calculations were made for orientation along the vertical axis. The optimal defocusing value for orientation measurements is $\sim -1 \mu\text{m}$. For that value, the bipolar character of the image is clearly discernible, but the fluorescence emission is not yet spread over an image area sufficiently large to severely worsen the signal-to-noise ratio, which is the case for larger defocusing values.

In our measurements we did not observe vertically oriented dipoles. This was so because the adsorbed dye molecules at an air-glass surface have a preferentially parallel orientation with respect to that surface. Furthermore, the Köhler illumination used in our setup does not have electric-field components perpendicular to the surface. Thus, for increasing inclination angle of the molecule's absorption dipole, the fluorescence excitation efficiency continually declines toward zero for a completely vertical dipole. If one is interested in observing mostly vertically oriented dipoles, one has to use a different mode of excitation, for example, excitation in total internal reflection as described in Ref. 28. However, as can be seen from Fig. 4, the images of a parallel-oriented di-

pole are most sensitive to defocusing, yielding different image topologies at different defocusing values. It is thus the best test sample when one is checking theory against experiment.

In conclusion, we emphasize that in this paper we have presented what is to our knowledge, the first complete and exact wave-optical calculation of defocused images of single emitting dipoles at an interface, having no recourse to any ray-tracing, scalar wave optical, or paraxial approximations and taking into account the exact angular distribution of radiation for an emitting dipole at an interface with a jump in refractive index. It should also be stressed that the calculations contain no adjustable parameter. The good agreement between theoretically calculated and experimentally measured images shows the high imaging quality of modern oil-immersion objectives, because the complete theoretical modeling as based on the Richards-Wolf approach relies heavily on the assumption of perfectly aplanatic imaging optics.

ACKNOWLEDGMENTS

We thank Francesco Pampaloni and David Raab for many helpful discussions and suggestions. We are much obliged to Benjamin Kaupp for his generous support of our research. We are grateful to the Deutsche Forschungsgemeinschaft (grant EN 297/7) for its financial support.

REFERENCES

1. C. Zander, J. Enderlein, and R. A. Keller, eds., *Single-Molecule Detection in Solution—Methods and Applications* (Wiley-VCH, Berlin, 2002).
2. J. Hofkens, W. Verheijen, R. Shulka, H. W. Schryver, and F. C. De, "Detection of a single dendrimer macromolecule with a fluorescent dihydropyrrroloporroledione (DPP) core embedded in a thin polystyrene film," *Macromolecules* **32**, 4493–4497 (1998).
3. C. Tietz, F. Jelezko, U. Gerken, S. Schuler, A. Schubert, H. Rogl, and J. Wrachtrup, "Single-molecule spectroscopy on the light-harvesting complex II of higher plants," *Biophys. J.* **81**, 556–562 (2001).
4. L. A. Deschenes and D. A. Van den Bout, "Single-molecule studies of heterogeneous dynamics in polymer melts near the glass transition," *Science* **292**, 233–234 (2001).
5. W. Trabesinger, A. Renn, B. Hecht, U. P. Wild, A. Montali, P. Smith, and C. Weder, "Single-molecule imaging revealing the deformation-induced formation of a molecular polymer blend," *J. Phys. Chem. B* **104**, 5221–5224 (2000).
6. A. Ishijima, H. Kojima, H. Higuchi, Y. Harada, R. Vale, T. Funatsu, and T. Yanagida, "Multiple-molecule and single-molecule analysis of the actomyosin motor by nanometer piconewton manipulation with a microneedle: unitary steps and forces," *Biophys. J.* **70**, 383–400 (1996).
7. K. Kinoshita, "Real time imaging of rotating molecular machines," *FASEB J.* **13**, S201–S208 (1999).
8. K. Kinoshita, "Linear and rotary molecular motors," *Adv. Exp. Med. Biol.* **453**, 5–14 (1998).
9. K. Kinoshita, H. Itoh, S. Ishiwata, K. Hirano, T. Nishizaka, and T. Hayakawa, "Dual-view microscopy with a single camera: real-time imaging of molecular orientations and calcium," *J. Cell Biol.* **115**, 67–73 (1991).
10. D. M. Warshaw, E. Hayes, D. Gaffney, A. M. Lauzon, J. R. Wu, G. Kennedy, K. Trybus, S. Lowey, and C. Berger, "Myosin conformational states determined by single fluorophore polarization," *Proc. Natl. Acad. Sci. (USA)* **95**, 8034–8039 (1998).

11. J. K. Trautman and J. J. Macklin, "Time-resolved spectroscopy of single molecules using near-field and far-field optics," *Chem. Phys.* **205**, 221–229 (1996).
12. J. J. Macklin, J. K. Trautman, T. D. Harris, and L. E. Brus, "Imaging and time-resolved spectroscopy of single molecules at an interface," *Science* **272**, 255–258 (1996).
13. W. P. Ambrose, P. M. Goodwin, J. C. Martin, and R. A. Keller, "Single-molecule detection and photochemistry of a surface using near-field optical excitation," *Phys. Rev. Lett.* **72**, 160–163 (1994).
14. A. G. T. Ruiter, J. A. Veerman, M. F. Garcia-Parajo, and N. F. Van Hulst, "Single-molecule rotational and translational diffusion observed by near-field scanning optical microscopy," *J. Phys. Chem. A* **101**, 7318–7323 (1997).
15. J. A. Veerman, M. F. Garcia-Parajo, L. Kuipers, and N. F. Van Hulst, "Single-molecule mapping of the optical field distribution of probes for near-field microscopy," *J. Microsc. (Oxford)* **194**, 477–482 (1999).
16. J. A. Veerman, S. A. Levi, F. C. J. M. Van Veggel, D. N. Reinhoudt, and N. F. Van Hulst, "Near-field scanning optical microscopy of single fluorescent dendritic molecules," *J. Phys. Chem. A* **103**, 11264–11270 (1999).
17. M. F. Garcia-Parajo, J. A. Veerman, G. M. J. Segers-Nolten, B. G. De Groot, J. Greve, and N. F. Van Hulst, "Visualizing individual green fluorescent proteins with a near-field optical microscope," *Cytometry* **36**, 239–246 (1999).
18. N. F. Van Hulst, J. A. Veerman, M. F. Garcia-Parajo, and L. Kuipers, "Analysis of individual (macro)molecules and proteins using near-field optics," *J. Chem. Phys.* **112**, 7790–7810 (2000).
19. M. A. Bopp, A. J. Meixner, G. Tarrach, I. Zschokke-Gränacher, and L. Novotny, "Direct imaging of single molecule diffusion in a solid polymer host," *Chem. Phys. Lett.* **263**, 721–726 (1996).
20. T. Ha, T. Enderle, D. S. Chemla, P. R. Selvin, and S. Weiss, "Single-molecule dynamics studied by polarization modulation," *Phys. Rev. Lett.* **77**, 3979–3982 (1996).
21. T. Ha, T. Enderle, D. S. Chemla, and S. Weiss, "Dual-molecule spectroscopy: molecular rulers for the study of biological macromolecules," *IEEE J. Sel. Top. Quantum Electron.* **2**, 1115–1128 (1996).
22. T. Ha, T. A. Laurence, D. S. Chemla, and S. Weiss, "Polarization spectroscopy of single fluorescent molecules," *J. Phys. Chem. B* **103**, 6839–6850 (1999).
23. R. A. Farrer, M. J. R. Previte, C. E. Olson, L. A. Peyser, J. T. Fourkas, and P. T. C. So, "Single-molecule detection with a two-photon fluorescence microscope with fast-scanning capabilities and polarization sensitivity," *Opt. Lett.* **24**, 1832–1834 (1999).
24. J. T. Fourkas, "Rapid determination of the three-dimensional orientation of single molecules," *Opt. Lett.* **26**, 211–213 (2001).
25. B. Sick, B. Hecht, and L. Novotny, "Orientational imaging of single molecules by annular illumination," *Phys. Rev. Lett.* **85**, 4482–4485 (2000).
26. M. A. Lieb and A. J. Meixner, "A high numerical aperture parabolic mirror as imaging device for confocal microscopy," *Opt. Express* **8**, 458–474 (2001), <http://www.opticsexpress.org>.
27. L. Novotny, M. R. Beversluis, K. S. Youngworth, and T. G. Brown, "Longitudinal field modes probed by single molecules," *Phys. Rev. Lett.* **86**, 5251–5254 (2001).
28. A. P. Bartko and R. M. Dickson, "Three-dimensional orientations of polymer-bound single molecules," *J. Phys. Chem. B* **103**, 3053–3056 (1999).
29. A. P. Bartko and R. M. Dickson, "Imaging three-dimensional single-molecule orientations," *J. Phys. Chem. B* **103**, 11237–11241 (1999).
30. R. M. Dickson, D. J. Norris, and W. E. Moerner, "Simultaneous imaging of individual molecules aligned both parallel and perpendicular to the optic axis," *Phys. Rev. Lett.* **81**, 5322–5325 (1998).
31. J. Jasny and J. Sepiol, "Single molecules observed by immersion mirror objective: a novel method of finding the orientation of a radiating dipole," *Chem. Phys. Lett.* **273**, 439–443 (1997).
32. J. Sepiol, J. Jasny, J. Keller, and U. P. Wild, "Single molecules observed by immersion mirror objective: the orientation of terrylene molecules via the direction of its transition dipole-moment," *Chem. Phys. Lett.* **273**, 444–448 (1997).
33. E. H. Hellen and D. Axelrod, "Fluorescence emission at dielectric and metal-film interfaces," *J. Opt. Soc. Am. B* **4**, 337–350 (1987).
34. J. Enderlein, T. Ruckstuhl, and S. Seeger, "Highly efficient optical detection of surface-generated fluorescence," *Appl. Opt.* **38**, 724–732 (1999).
35. J. D. Jackson, *Classical Electrodynamics* (Wiley, New York, 1975).
36. J. Enderlein, "Theoretical study of detecting a dipole emitter through an objective with high numerical aperture," *Opt. Lett.* **25**, 634–636 (2000).
37. B. Richards and E. Wolf, "Electromagnetic diffraction in optical systems. II. Structure of the image field in an aplanatic system," *Proc. R. Soc. London Ser. A* **235**, 358–379 (1959).
38. M. Abramowitz and I. A. Stegun, eds., *Handbook of Mathematical Functions* (Harry Deutsch, Frankfurt/Main, Germany, 1984).